In Situ EXAFS Study of the Photocatalytic Reduction and Deposition of Gold on Colloidal Titania

ARTICLE *in* THE JOURNAL OF PHYSICAL CHEMISTRY · MARCH 1995

Impact Factor: 2.78 · DOI: 10.1021/j100010a047

In Situ EXAFS Study of the Photocatalytic Reduction and Deposition of Gold on Colloidal Titania

A. Fernández,* A. Caballero, and A. R. González-Elipe

Instituto de Ciencia de Materiales de Sevilla (CSIC-Universidad de Sevilla) and Departamento de Química Inorgánica, Apartado 1115, 41080 Sevilla, Spain

J.-M. Herrmann

URA au CNRS "Photocatalyse, Catalyse et Environnement", Ecole Centrale de Lyon, B.P. 163, 69131 Ecully Cedex, France

H. Dexpert and F. Villain

Laboratoire pour l'Utilisation du Rayonnement Electromagnetique (LURE), F-91405 Orsay Cedex, France

Received: August 9, 1994; In Final Form: October 27, 1994[⊗]

The photocatalytic reduction of gold on a colloidal TiO_2 sample in the presence of *i*-PrOH has been studied by in situ EXAFS. This colloidal sample shows a quantum size effect in its band gap UV−vis absorption and a photocatalytic activity for the formation of Ti^{3+} species. An experimental setup has been used that consists of a photochemical reactor connected to a peristaltic pump and an EXAFS transmission cell specially designed for liquid samples. The results show that it is possible to follow the two-step mechanism of the photoreduction of noble metals on titania, i.e. the nucleation and the growth of the metallic crystallites. At the same time, a surprisingly low intensity of the threshold feature at the Au L_{III} edge has been found for low irradiation times, when small gold particles are formed. This effect has been interpreted as a result of a negative charge injection into the metal particles which is favored by the presence of the alcohol acting as a hole trap. For comparison, an in situ XPS analysis has been carried out to follow the photoreduction of gold in a Au^{3+}−TiO_2 material in the presence of *i*-PrOH at the gas−solid interface.

Introduction

Metal cations with the appropriate redox potentials can be reduced at room temperature by photoelectrons created by band gap illumination of common semiconductors. The noble metals usually photodeposited are Pt, Pd, Rh, Au, Ir, and Ag, and they have been photoreduced on various semiconductors, mainly oxides such as ZnO, WO_3, and predominantly TiO_2 (refs 1−10 and references therein). This process has a great interest because of its potential applications in (i) the recovery of noble metals,[7,11] (ii) the metalization processes by wet methods,[12] (iii) the elimination of heavy metals from waste water,[13] or (iv) the synthesis of M/TiO_2 materials which can be employed as catalysts or as chemical sensors.[6,8] However, in spite of the number of papers already published, more work is needed to clarify the mechanism by which crystallites of metal are formed during the photoreduction process. In a previous paper,[14] we have studied by XPS (X-ray photoelectron spectroscopy) the photocatalytic reduction of Rh^{3+}, Pt^{4+}, Pd^{2+}, and Ag^+ on TiO_2, showing the influence of the mass transport phenomena in the final size of the metallic crystallites.

The EXAFS (extended X-ray absorption fine structure) technique is a powerful structural tool that gives information on interatomic distances and coordination numbers.[15−16] The technique is extremely fast by using synchrotron radiation; it can be used for amorphous solids or solutions, and it is sensitive to the local environment to the specific absorbing atom.[15,16] In a previous paper J. W. W. Jacobs et al.[17] have studied by HREM and EXAFS the photodeposition of copper on TiO_2 from an alkaline electroless copper solution. In the present paper we have used this valuable technique to study in situ the photocatalytic reduction of gold on colloidal TiO_2 in an aqueous/alcoholic solution. Important conclusions on the reaction mechanism have been drawn from the experimental results which were compared with those obtained by XPS, during the irradiation of a pressed pellet of a Au^{3+}−TiO_2 composite material in the presence of *i*-PrOH/H_2O in the gas phase. This comparison enabled us to analyze the influence of the liquid−solid and the gas−solid interfaces in the mechanism of the photodeposition of noble metals on semiconductors.

Experimental Section

(i) Photochemistry of Colloidal TiO_2. For the preparation of the colloidal TiO_2 solution, 80 mL of titanium tetraisopropoxide ($Ti(OCH(CH_3)_2)_4$) from Merck was added dropwise into a solution formed by 40 mL of *i*-PrOH and 180 mL of HCl (2 mol·L^{-1}). Although sometimes the solution became a little turbid during the addition of the alcoholate, the turbidity disappeared after stirring for a few minutes. As a result of the hydrolysis of the alcoholate, we obtained a colloidal TiO_2 solution with a concentration ca. 0.9 M.

For the photoreduction experiments, 1.76 g of $HAuCl_4 \cdot 3H_2O$ (Aldrich) dissolved in 10 mL of water was added to 300 mL of the colloidal TiO_2 solution. The content in Au^{3+} remaining in solution after the photoreduction of gold and the flocculation of the colloid was measured by atomic absorption spectroscopy, and a reduction rate of 98% was determined, which corresponded to a final metal loading of ca. 4% by weight. Although higher amounts of gold can be easily photoreduced on titania, this value of 4% was selected to have enough accuracy and sensitivity in the EXAFS spectra, especially in

[⊗] Abstract published in *Advance ACS Abstracts,* January 15, 1995.

0022-3654/95/2099-3303$09.00/0

the initial period of the photoreaction, to get information on the first steps of the photoreduction processes.

Illumination was provided by a high-pressure mercury lamp (Philips HPK, 125 W) in an immersion cell for photochemical reactions made of fused silica. The solution was purged with argon before irradiation in order to avoid the photoadsorption of oxygen.

(ii) EXAFS Measurements. The experimental setup for in situ EXAFS analysis of photochemical reactions has been described in detail elsewhere.[18] It consists of an immersion cell for irradiation attached to a peristaltic pump. By this way, the aqueous suspension was pumped out during illumination from the reaction vessel to a conventional transmission cell with variable thickness located in the beam and described elsewhere.[19]

The measurements were carried out at the XAS3 line at the LURE Synchrotron, having a double crystal Si(111) monochromator with a resolution at the Au L_{III} edge of about 1 eV. This line is equipped with a fast acquisition facility[20,21] that allows one to record a XAS spectrum at 298 K with a mean ring current of about 200 mA (ring current after injection: 300 mA, lifetime > 100 h) in ca. 1−2 min. More than 20 spectra were recorded at different irradiation times during the time necessary for the total photoreduction of gold (about 4 h with the conditions of illumination used). The XANES and EXAFS regions were recorded in two separated spectra on the same sample. The reference spectra of the metallic gold foil and of the $AuCl_4^-$ solution were recorded in exactly the same conditions as the in situ experiments.

It should be emphasized that, in order to get a good signal to noise ratio in the spectra, the concentrations of the reactants have been adjusted to provide an appreciable absorption edge (ca. 0.15 absorbance units) of the element that we want to monitor (in this case the Au L_{III} edge) in relation to the total absorption of the reaction solution (i.e. TiO_2, H_2O, Au, and Cl).[18] On the other hand, the most commonly used system for the study of the photodeposition of noble metals on titania consists of illuminating a TiO_2 aqueous suspension. However, in this work we have carried out the experiments on a homogeneous colloidal TiO_2 solution to avoid the dispersion of the light during the recording of EXAFS spectra, thus improving the quality of the data.[18]

The spectra were analyzed with the software package developed by Bonin et al.[22] The Fourier transforms have been carried out between 2.5 and 13.0 $Å^{-1}$ with a Kayser type window using a τ factor of 4.5 and multiplied by a k^3 factor. The coordination numbers (CN), distances (R), and Debye−Waller ($\Delta\sigma$) values were extracted by a least-squares fitting procedure that makes use of the phase and amplitude extracted from the appropriate model compounds (Au foil and $HAuCl_4$).

(iii) TEM Analysis. The TEM examination of the samples was carried out on a Hitachi H800 microscope working at 200 kV. For the preparation of the samples, the colloidal solution obtained after illumination (which was partially flocculated) was passed through a polyvinyl filter. The filter was sonicated in ethanol, and a drop of the obtained suspension was deposited on a thin carbon film supported by a copper grid.

STEM-EDX analysis was performed with an STEM field-emission gun (VG HB 501) equipped with a silicon−lithium diode detector (Link) and a multichannel analyzer (Tracor 5500).

(iv) XPS Measurements. The Au^{3+}−TiO_2 sample was prepared by incipient wetness impregnation of the powdered anatase (TiO_2 Degussa P-25, S_{BET} = 50 $m^2 \cdot g^{-1}$) with a $HAuCl_4 \cdot 3H_2O$ (Aldrich Chem) aqueous solution, corresponding to a metal loading of 4% by weight.

The illumination was carried out in the pretreatment chamber of the XPS spectrometer in which the samples, in the form of pressed pellets (7 × 7 mm^2), were irradiated in the presence of 3×10^{-1} Torr of the vapor pressure of an *i*-PrOH/H_2O (v/v, 1:1) mixture, as previously described.[14] Illumination was carried out through a Pyrex window using the light of a high-pressure Hg lamp (Philips HPK 125 W) focused with a lens on top of the sample holder so that the complete sample area was irradiated. A water filter for IR radiation was used in the experiments to avoid additional heating of the sample.

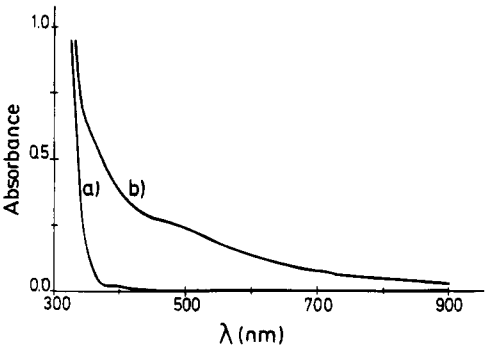

Figure 1. Absorption spectra of the original TiO_2 colloidal sample (a) and after irradiation and exposition to air for 15 min (b).

For comparison, thermal reduction of the Au^{3+}−TiO_2 material was carried out in the pretreatment chamber of the XPS spectrometer by heating the sample in H_2 (10 Torr) at 473 K.

XPS spectra were recorded with a Leybold−Heraeus LHS-10 spectrometer using Mg Kα radiation as the excitation source and a pass energy of 50 eV. Binding energy (BE) reference was taken at the Ti $2p_{3/2}$ peak of Ti^{4+} at 458.5 eV. Sensitivity factors supplied with the instrument were employed to calculate the atomic percentages.

Results

1. Preliminary Evidence for the Photocatalytic Activity of Colloidal TiO_2. For this in situ EXAFS study we have selected a colloidal TiO_2 solution to improve the quality of the spectra by working in a homogeneous medium (absence of dispersion and/or refraction of the light). For this reason we have tested in a first step the optical absorption and the photocatalytic properties of the colloidal titania sample. In this respect, Figure 1 shows the UV−vis absorption spectrum of the TiO_2 colloidal solution from which we have evaluated the band gap of the sample by plotting $(\text{absorbance} \cdot h\nu)^2$ (where $h\nu$ is the photon energy) against $h\nu$. The extrapolation of the linear portion of the curve to zero absorption[23] provided a value of 3.7 eV for the band gap, substantially different from the value of 3.2 eV found in the literature for bulk anatase TiO_2.[24] This blue shift in the band gap is characteristic of colloidal TiO_2 particles of very small size[25] and has been attributed to a quantum size effect.[26] Illumination of the colloidal solution in the absence of oxygen leads to the evolution of a blue-violet color that disappears after 2 h of exposition of air and is likely due to the generation under irradiation of Ti^{3+} species.[27] This effect clearly shows the photoactivity of the colloid so that, under band gap illumination, the photogenerated holes are trapped by the *i*-PrOH,[28] which is finally oxidized into acetone while the photoelectrons induce the formation of the Ti^{3+} species.

In addition, we have depicted in Figure 1 the UV−vis spectrum obtained for the illuminated TiO_2 colloid after 15 min of air exposure (the time necessary for taking the sample from the reaction vessel and recording the optical absorption spectra). The sample still exhibits some blue color and the apparition of

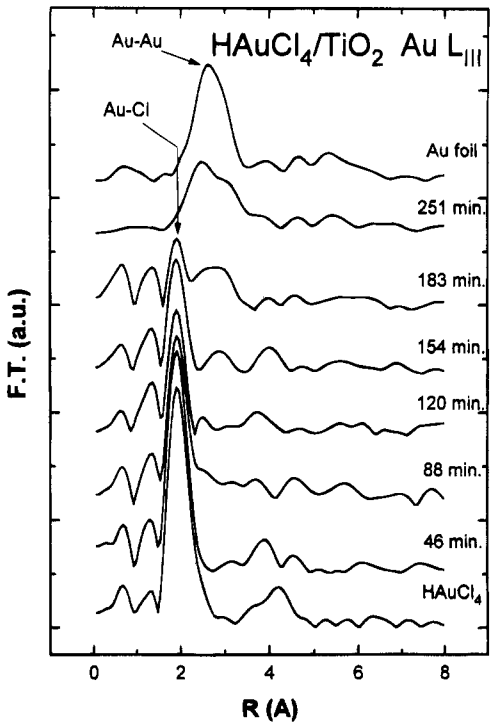

Figure 2. Modulus of the Fourier transform of the Au L_{III} edge recorded at different illumination times during the photocatalytic reduction of Au^{3+} on a colloidal TiO_2.

an absorption band between 400 and 500 nm. This absorption band is attributed to the formation of peroxide species due to the reaction of the blue Ti^{3+} centers with oxygen as follows:[25]

$$TiO_2(Ti^{3+}) + O_2 \rightarrow TiO_2{-}O_2^{\bullet -} + Ti^{4+} \qquad (1)$$

In fact, the titanyl−peroxide reaction yielding a yellow complex is a well-established method for the quantitative analysis of H_2O_2,[29] and it has been shown that μ-peroxo complexes on TiO_2 surfaces are formed upon photoadsorption of O_2.[30] In our case the spectrum in Figure 1 indicates that under band gap illumination reducing equivalents are stored on the semiconductor colloidal particles, which enables a subsequent thermal reaction to form such peroxo complexes. In conclusion all these results show that in acidic medium and in the presence of *i*-PrOH as a hole scavenger the colloidal TiO_2 sample appears suitable for the study of photoreduction reactions and, in particular, for the study of the photoreduction of gold as described below.

2. In Situ EXAFS Study of Au Photodeposition. Once we established the photocatalytic activity of the colloidal TiO_2 sample, we registered the EXAFS region of the Au L_{III} edge spectra at different illumination times during the photocatalytic reduction of Au^{3+} in the alcoholic colloid solution. The quality of the data was very good even if some turbidity, due to a partial flocculation of the colloid, appeared during the experiment. The Fourier transforms (FT) of the EXAFS oscillations[15−17] obtained for the different illumination times and for a foil of gold are represented in Figure 2. The first peak in the FT spectra corresponds to the Au−Cl distance for the $AuCl_4^-$ anions initially present in the solution (time zero of irradiation), while the second peak corresponds to Au−Au distances in the first coordination shell of metallic gold. Fitting analyses of the Fourier transforms depicted in Figure 2 are summarized in Table 1. We found a Au−Cl distance of 2.28 Å with an initial coordination number (N_{Au-Cl}) of 4, corresponding to pure $(AuCl_4)^-$ species. As photoreduction proceeds, the number of Au−Cl bonds progressively decreases and reaches 0 when the total reduction is achieved. By assuming (i) that gold species still oxidized are present as $AuCl_4^-$ and (ii) that the decrease of the coordination number from its initial value of 4 is due to the reduction to Au^0, it was possible to calculate the percentage of Au^0 formed:

$$Au^0\ \% = [(CN(Cl))_0 - (CN(Cl))]/(CN(Cl))_0$$

In a previous paper by J. W. H. Jacobs et al.,[17] the formation of partially reduced Cu^+ species (as Cu_2O) has been demonstrated during the photochemical reduction of Cu^{2+} on titania from an alkaline electroless copper solution. However, in the present study, the presence of Au^+ species has not been taken into account due to the instability of such species in acidic solutions.[31]

In relation to the peak in the FT corresponding to the Au−Au distances, it is important to note that although the peak corresponding to the Au−Cl distances strongly diminishes in intensity from the beginning of illumination, we start to detect clearly the Au−Au distances only after long periods of irradiation (154 min). The fitting analysis of the Au−Au coordination bond obtained for these long irradiation periods gave a distance value of 2.87 Å and a coordination number that increases up the final value of 12, corresponding to the bulk one found in big particles of gold. To take into account that only reduced gold contributes to the Au−Au coordination sphere, a corrected coordination number ($N'_{Au-Au} = N_{Au-Au} \times 100/Au^0\ \%$) has been calculated and included in Table 1. From these values it is clear that even after 154 and 183 min of illumination very small clusters of gold are formed, which correspond to N'_{Au-Au} values smaller than 12. In fact, when small metal clusters are examined by EXAFS, the apparent mean coordination number is smaller than that observed in bulk metal because of the high proportion of surface atoms (high metal dispersion). In addition the formation of highly dispersed metallic gold will lead to a weak signal and a very large Debye−Waller factor due to the lack of crystallization in the very small particles. These small particles will then progressively grow under illumination to form crystallites presenting the full coordination number of gold. Here it should be noted that the

TABLE 1: Best Fitting Parameters for the EXAFS Function of the First Coordination Shell of Gold during the Photocatalytic Reduction of $(AuCl_4)^-$ on Colloidal TiO_2[a]

time (min)	NN	CN	R	$\Delta\sigma$	ΔE_0	Au^{3+} %	Au^0 %	N'_{Au-Au}
0	Cl	4.0	2.28	0.0	0.0	100	0	
	Au	0.0						
46	Cl	3.6	2.28	0.0	0.77	90	10	
	Au	0.0						
88	Cl	2.9	2.28	0.0	−0.45	73	27	
	Au	0.0						
120	Cl	2.1	2.28	0.0	−0.58	53	47	
	Au	0.0						
154	Cl	1.76	2.28	0.0	0.69	44	56	6.2
	Au	3.5	2.87	0.067	−0.58			
183	Cl	1.15	2.28	0.0	−0.82	29	71	10.4
	Au	7.4	2.87	0.054	−0.57			
251	Cl	0.0				0	100	12
	Au	12	2.88	0.005	0.67			

[a] Estimated precision: CN ±15%, R ±0.02 Å, $\Delta\sigma$ ±20%. NN type of atom in the first coordination shell of gold. CN, coordination number. R, distance in Å. $\Delta\sigma$, Debye−Waller factor in angstroms relative to the foil of gold or the $AuCl_4^-$ solution. ΔE_0, shift of E_0 value. Au^{3+} %, percentage of remaining $(AuCl_4)^-$ species calculated as $100N_{Au-Cl}/4$. Au^0 %, percentage of reduced gold calculated as 100 − Au^{3+} %. N'_{Au-Au}, coordination number for reduced gold corrected by taking into account the degree of reduction ($N'_{Au-Au} = 100N_{Au-Au}/Au^0$ %).

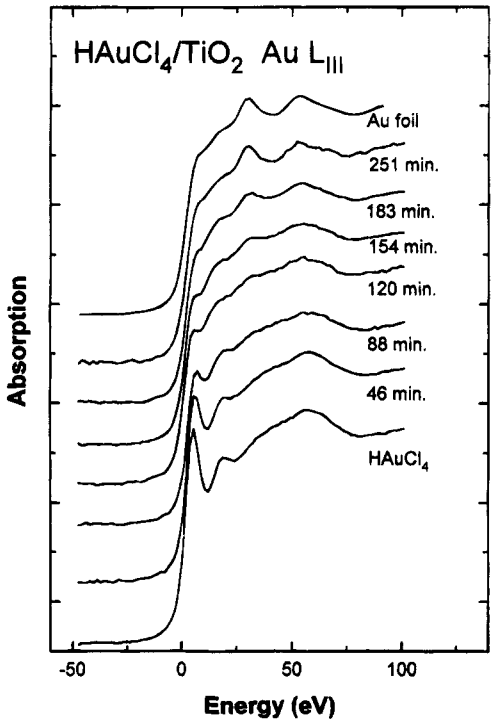

Figure 3. XANES region spectra of the Au L_{III} edge recorded at different illumination times during the photocatalytic reduction of Au^{3+} on a colloidal TiO_2.

coordination number for the Au−Au distance obtained for the irradiation time of 154 min is influenced by a high error due to the very small Au−Au signal obtained for these situations. Furthermore, standard EXAFS analysis of clusters underestimates the coordination number[32] so that the estimated precision of ±15% is justified in this case. Also it is important to note that the complex behavior[15] of the backscattering amplitude function for gold gives rise to a complex profile for the gold−gold peak in the Fourier transforms. For this reason the two peaks appearing between 2.0 and 3.5 Å in Figure 2 correspond to the first coordination shell of gold in the metallic particles.

3. XANES Study of Photodeposited Gold. We have simultaneously registered the XANES regions of the Au L_{III} absorption edge. In Figure 3, we can clearly observe an important decrease in the intensity of the threshold resonance for this edge during illumination, which shows the progressive reduction of the Au^{3+} species. In fact the white line of L_{II} and L_{III} edges is due to spectroscopic transitions from 2p to d vacant states and can be related to the local density of d vacant states in metal atoms[33] or equivalently to the degree of reduction of the metal. No considerations about the chemical state of gold have been inferred from the position of the edge.

To correlate the degree of reduction calculated from the EXAFS data (Table 1) with the observed changes in the XANES spectra, we have depicted in Figure 4 a linear combination of the spectra of a gold foil and of the initial $HAuCl_4$ solution according to the Au^0 and Au^{3+} percentages given in Table 1. The comparison of the calculated spectra with the experimental ones at different UV irradiation times (Figure 4) shows a good agreement in the oscillations feature of the XANES region (above 12 eV), except for the value of the intensity of the first feature on the edge, which is always smaller than the calculated one. This surprising effect, which will be discussed further, was confirmed by the results presented in Figure 5, where we have depicted the XANES region spectra obtained for the longest UV irradition times superimposed on the spectrum of the gold foil. The height of the threshold resonance is equivalent

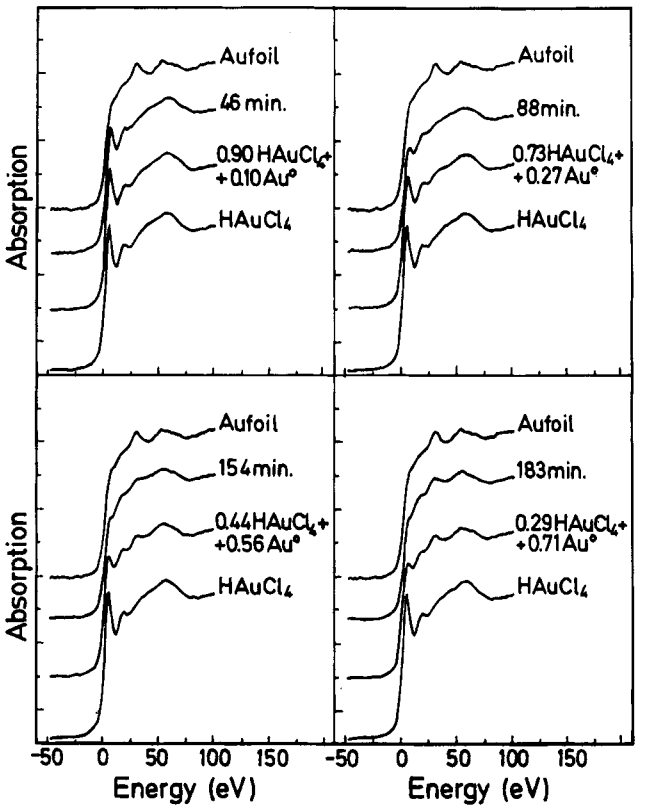

Figure 4. XANES region spectra of the Au L_{III} edge recorded at different UV illumination times (46, 88, 154, 183 min) compared with linearly combined spectra of a gold foil and of the initial $HAuCl_4$ solution.

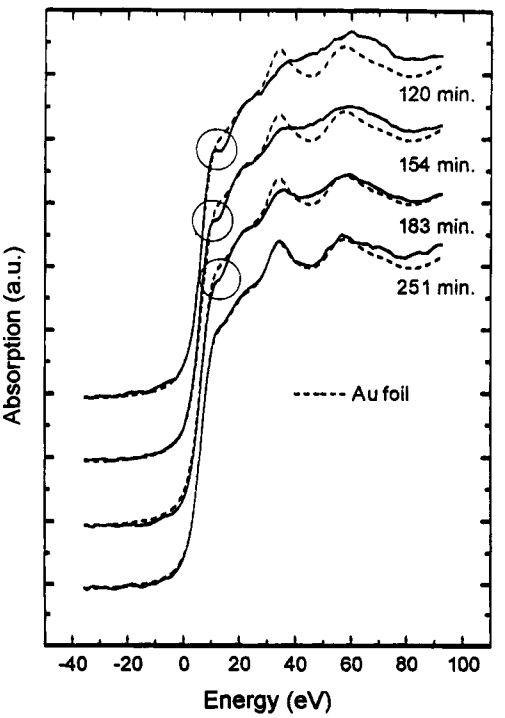

Figure 5. Superposition of the XANES region spectra of the Au L_{III} edge recorded at different UV illumination times and of the spectrum of the gold foil.

to that of the gold foil only after 251 min of UV irradiation. It is smaller in the other cases. This is indicative of a smaller density of d vacant states or similarly of a reduction state of the sample higher than that of the gold foil. This effect confirms again the unexpected decrease of the intensity of the threshold

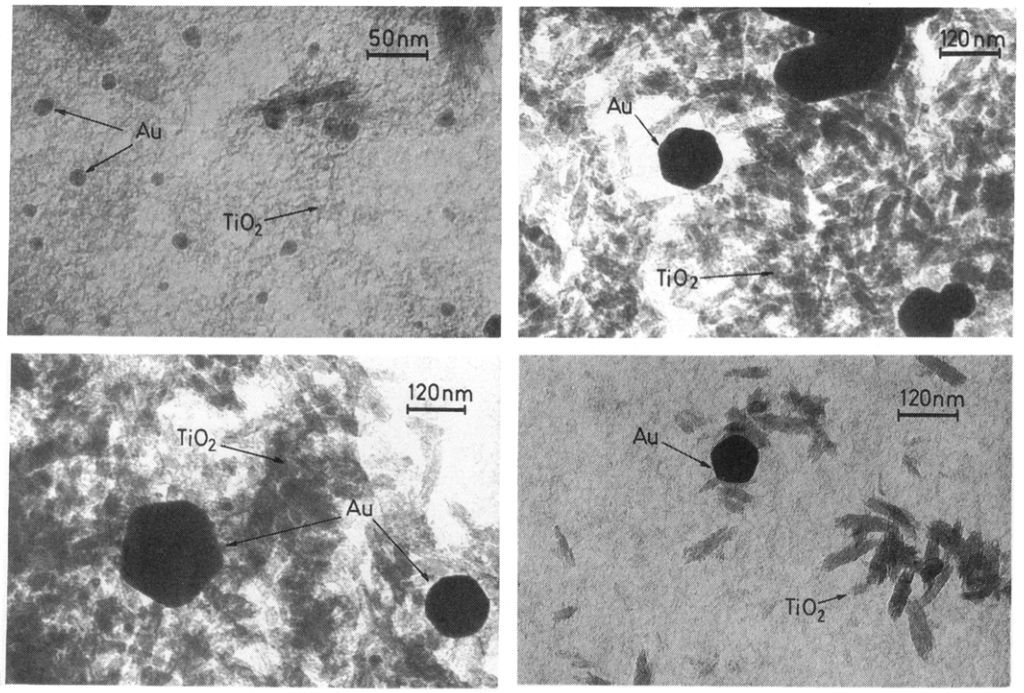

Figure 6. Transmission electron micrographs of the partially flocculated TiO_2 colloid after total reduction of gold.

resonance line even in the cases where still some Au−Cl bonds remain detected in the Fourier transforms due to the presence of Au^{3+} species. In addition we should emphasize that in order to get a good agreement in the intensity of the first feature at the edge we can make a linear combination of the Au^{3+} and Au^0 spectra involving a higher contribution of Au^0 than that expected from the EXAFS data in Table 1, but in this case no agreement is obtained for the XANES region above 12 eV.

4. TEM Examination. The TEM examination (Figure 6) of the colloid obtained after 251 min of UV irradiation shows the presence of a porous structure that corresponds to the partially flocculated TiO_2 colloidal particles together with big particles of gold. The size of the Au crystallites is rather heterogeneous, ranging from 6 to 200 nm. In fact, most of the metallic gold appears finally as a few very big particles (100−200 nm) besides the presence of smaller ones (≥6 nm). The presence of small particles (<6 nm) which could not be distinguished because of the porous structure of the TiO_2 phase has been discarded by STEM analysis of the regions free of gold crystallites.

5. Complementary XPS Study. Finally we have carried out a similar experiment by illuminating a $Au^{3+}-TiO_2$ sample in the form of pressed pellets in the presence of *i*-PrOH/H_2O in the gas phase and following by XPS[14] the Au 4f photoelectron doublet peak. The aim of this experiment was to compare the growth mechanism during the formation of the gold crystallites in an aqueous/alcoholic liquid medium or in the presence of *i*-PrOH/H_2O at the gas−solid interface. The results summarized in Figure 7 show that initially and under the ultrahigh vacuum conditions of the spectrometer it is possible to stabilize Au^+ species that photoreduce into Au^0 immediately under illumination. It is interesting to note that after short irradiation times the BE value for the Au $4f_{5/2}$ peak is about 0.3 eV higher than that obtained for longer illumination times. This shift can be interpreted as a size effect which is usually observed in metal-supported catalysts.[33] These results were further confirmed by the quantitative XPS analysis of the spectra: if we take 100% for the normalized intensity (normalization to the intensity of the Ti2p peak) of the Au 4f photoelectron peak of the original sample, a value of 79% is obtained for the sample illuminated

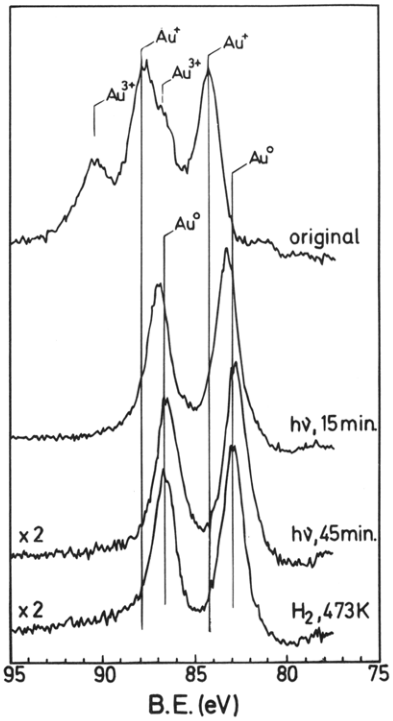

Figure 7. Evolution in the dark and under UV illumination of the Au (4f) photoelectron peak of the $Au^{3+}-TiO_2$ precursor material.

for 15 min and a value of 36% for the other two samples, i.e. the one which has been illuminated for 45 min and the other which has been thermally reduced. The decrease in the area of the Au 4f photoelectron peak confirms the agglomeration of the metal into bigger particles. It is important to mention that UV illumination of the same $Au^{3+}-TiO_2$ precursor in a suspension of *i*-PrOH/H_2O at pH = 2 leads to a fully reduced $Au-TiO_2$ sample which gives by XPS a normalized intensity for the Au 4f peak equal to 7% of the signal obtained for the original sample. This indicates, in the case of UV irradiation in a liquid medium, the formation of metal particles bigger than those obtained at a gas−solid interface.

Discussion

The in situ EXAFS analysis presented in this paper is summarized in the FTs represented in Figure 2. It is clear from this figure and from the data in Table 1 that the Au−Cl distances start to disappear without the simultaneous growth of the Au−Au distances, which begin to appear only after illumination for 154 min. The continuous decrease in the intensity of the first feature at the edge of the XANES region indicates, however, a progressive reduction of the Au^{3+} during the experiment. These results are particularly interesting because they provide a direct observation in real time of a two-step mechanism (i.e. nucleation and growth) of the photocatalytic reduction of noble metals on titania under band gap illumination. During the first step a reduction−nucleation process will occur in which some Au^{3+} ions are reduced to Au^0. The size of the Au clusters generated during this initial step is small so that no detectable Au−Au distances corresponding to a metallic phase could be obtained from the FTs. Once the clusters have reached a critical size, the growth step begins to generate bigger particles of gold with a metallic character. This interpretation is congruent with previous results in the literature,[6,11,35] so that the following mechanism has been postulated:

(1) Generation of electron-hole pairs by UV-light absorption,

$$TiO_2 \xrightarrow[\lambda_{exc} < 380\ nm]{h\nu} TiO_2(h^+_{VB}, e^-_{CB}) \quad (2)$$

(2) Reduction by the semiconductor free electrons of the metal cations into zerovalent atoms,

$$Au^{3+} + 3(e^-_{CB}) \rightarrow Au^0 \quad (3)$$

(3) Simultaneous oxidation of the alcohol by the photoproduced holes,

$$CH_3{-}CHOH{-}CH_3 + h^+_{VB} \rightarrow CH_3{-}\dot{C}HO{-}CH_3 + H^+ \quad (4)$$

(the alcohol radical will further react)

(4) Spontaneous agglomeration of zerovalent metal atoms into small crystallites via two possible processes: either a single metal atom migration,

$$mAu^0 \rightarrow Au_m \text{ (supported)} \quad (5)$$

or a cathodic-like reduction at primary metallic nuclei,

$$Au + Au^{3+} \rightarrow (Au_2)^{3+} \xrightarrow{+3e^-} Au_2 \xrightarrow{+Au^{3+}} (Au_3)^{3+} \xrightarrow{+3e^-} Au_3 \rightarrow \ldots \rightarrow Au_m \quad (6)$$

A careful and detailed STEM analysis of the final colloid shows the absence of very small gold particles. This indicates that the very small Au^0 clusters constitute an initial transient situation. The growth of the big crystallites is correlated with the elimination of the very small clusters initially formed. This effect was later confirmed by XPS analysis which indicates, even at short irradiation times, a fully reduced gold phase, whereas a prolonged UV illumination produced a decrease in the intensity of the gold photoelectron peaks, corresponding to an agglomeration of the particles. This diminution is extremely important in the case of the illumination of the colloid in an aqueous/alcoholic suspension, where is it possible that the very small Au^0 clusters could be dissolved and reduced again on a particle which is growing according to a cathodic-like reaction (6).

It is also important to remark that the intensity of the threshold resonance of the XANES spectra shows a singular behavior for the situations in which the mean particle size is very small (at least up to 11 Å). Under these conditions a peak smaller than that of bulk metallic gold (Figures 5 and 6) indicates a smaller density of vacant d states in the metallic particles. This should correspond to a negative charge injection in the clusters, this effect being undetectable in the case of big crystallites of gold. In fact, only for small Au^0 particles does the excess of negative charge have an influence on the XANES region. For big particles the number of gold atoms is so high that the charge is distributed and no significant effects are detected. Similar effects have been observed by S. McCuaing et al.[36] in the near edge structure of Au−Te alloys.

To understand this effect, we can think in the experiment of the TiO_2 colloid in the absence of Au^{3+}, where we have clearly detected the formation of Ti^{3+} or reducing equivalents under illumination. At the same time in the alcoholic medium, the photoproduced alcohol radical in reaction 4 can also react with the colloid according to

$$TiO_2(Ti^{4+}) + CH_3{-}\dot{C}HO{-}CH_3 \rightarrow TiO_2(Ti^{3+}) + CH_3{-}CO{-}CH_3 + H^+ \quad (7)$$

This reaction has been observed for the radicals generated during the γ-irradiation of alcohols[27a] and leads to a current doubling effect. All these mechanisms generate Ti^{3+} or reducing equivalents highly stabilized for the colloidal sample in the alcoholic medium, as shown by the persistence of the blue color for an irradiated TiO_2 colloidal sample in the absence of O_2. This phenomenon is identical to that observed on TiO_2 Degussa P-25 (anatase) in the photocatalytic dehydrogenation of $C_1{-}C_4$ aliphatic alcohols.[28] Presently, the photoproduced electrons not only reduce $AuCl_4^-$ into Au^0 but also contribute to an electron injection in the small Au particles initially formed. Such a phenomenon does not occur with small metal particles supported on insulators, such as alumina or silica, for which, by contrast, an increase of the threshold resonance intensity is observed.[37]

Actually, the decrease in the intensity of the first feature at the edge of the XANES region for titania-deposited metals is supported by previous photoconductivity measurements, which provided evidence for a spontaneous electron transfer from the support to the metal either under vacuum, in reducing conditions,[38] or in an oxygen atmosphere.[39] This electron transfer is the consequence of the increase of the Fermi level of titania under illumination and of the subsequent alignment of the Fermi levels of both phases (metal and support). The overall electron transfer becomes more important as the amount of the deposited metal increases, since the steady state photoconductivity of M/TiO_2 samples varies conversely with the metal content.[38,39]

Presently, the same type of electron transfer occurs from colloidal titania to gold clusters and explains the abnormally small intensity of the threshold resonance line in the XANES region in Figure 5. Additionally, this electron transfer accounts for the cathodic-like reduction of eq 6 and explains why a small crystallite can grow at the surface of UV-illuminated titania in the presence of a metal solution.

Conclusions

In the present paper we have directly observed in real time the nucleation and growth mechanism for the formation of metallic crystallites during the photoreduction of noble metal cations on semiconductor materials. It is clear from the results presented above that only a few of the metallic nuclei initially

formed will grow to form big crystallites, this effect being enhanced by working in a liquid medium. In addition, a negative charge injection from the colloidal semiconductor to the small metallic clusters has been postulated to explain the surprisingly low intensity of the first feature at the edge of the Au L_{III} absorption. This charge transfer is in agreement with previous photoconductivity measurements. On the other hand, the EXAFS study presented above illustrates the potentiality of the experimental setup for the study of photochemical and photocatalytic reactions by working in homogeneous media. Finally, it is important to emphasize the possibility of following in real time the process of the photodeposition of gold even though the EXAFS analysis provides information which is the average of the gold signal in the reaction solution.

Acknowledgment. The authors thank the DGICYT (Project No. PB91-0835 and PB93-0183) and the LIP (Large Installation Program) of the EEC for financial support. The facilities given by LURE, the "Servicio de Microscopía Electrónica de la Universidad de Sevilla", and C. Leclercq (Institut de Recherches sur la Catalyse, Lyon, STEM analysis) are also acknowledged.

References and Notes

(1) Krauetler, B.; Bard, A. J. *J. Am. Chem. Soc.* **1978**, *100*, 4317.
(2) Stadler, K. H.; Boehm, H. P. In *Proceedings of the 8th International Congress on Catalysis, Berlin, Vol. IV*; Verlag Chemie: Weinheim, 1984; p 803.
(3) Sato, S. *J. Catal.* **1985**, *92*, 11.
(4) Nakamatsu, H.; Kawai, T.; Koreeda, A.; Kawai, S. *J. Chem. Soc., Faraday Trans. 1* **1985**, *82*, 527.
(5) Borgarello, E.; Serpone, N.; Emo, G.; Harris, R.; Pellizzetti, E.; Minero, C. *Inorg. Chem.* **1986**, *25*, 4499.
(6) Herrmann, J.-M.; Disdier, J.; Pichat, P.; Leclercq, C. In *Preparation of Catalysts IV*; Delmond, B., Grange, P., Jacobs, P. A., Poncelet, G., Eds.; Elsevier: Amsterdam, 1987; p 285.
(7) Herrmann, J.-M.; Disdier, J.; Pichat, P. *J. Catal.* **1988**, *113*, 72.
(8) (a) Fernández, A.; Munuera, G.; González-Elipe, A. R.; Espinós, J. P.; Herrmann, J.-M.; Pichat, P.; Leclercq, C. *Appl. Catal.* **1990**, *57*, 191. (b) Herrmann, J.-M.; Disdier, J.; Pichat, P.; Fernández, A.; González-Elipe, A. R.; Munuera, G.; Leclercq, C. *J. Catal.* **1991**, *132*, 490.
(9) Jacobs, J. W. M.; Schryvers, D. *J. Catal.* **1987**, *103*, 436.
(10) Hada, H.; Yonezawa, Y.; Ishino, M.; Tanemura, H. *J. Chem. Soc., Faraday Trans. 1* **1982**, *78*, 2677.
(11) Herrmann, J.-M.; Disdier, J.; Pichat, P. *J. Phys. Chem.* **1986**, *90*, 6028.
(12) (a) Harada, Y.; Fushimi, K.; Madokoro, S.; Sawai, H.; Ushio, S. *J. Electrochem. Soc.* **1986**, *113*, 2428. (b) Sausa, R. C.; Cripta, A.; White, J. R. *J. Electrochem. Soc.* **1987**, *134*, 2707.
(13) Tanaka, K.; Harada, K.; Murata, S. *Solar Energy* **1986**, *36*, 159.
(14) Fernández, A.; González-Elipe, A. R. *Appl. Surf. Sci.* **1993**, *69*, 285.
(15) Köningsberger, D. C., Prins, R., Eds. *X-Ray Absorption: Principles, Applications, Techniques of EXAFS, SEXAFS and XANES;* John Wiley & Sons: New York, 1988.
(16) (a) Teo, B. K., Joy, D. C. Eds. *EXAFS Spectroscopy. Techniques and Applications*; Plenum Press: New York, 1981. (b) Teo, B. K. *EXAFS: Basic Principles and Data Analysis*; Springer Verlag: New York, 1986.
(17) Jacobs, J. W. M.; Kampers, F. W. H.; Rikken, J. M. G.; Bulle-Lieuwma, C. W. T.; Koningsberger, D. C. *J. Electrochem. Soc.* **1989**, *136*, 2914.
(18) Caballero, A.; González-Elipe, A. R.; Fernández, A.; Herrmann, J.-M.; Dexpert, H.; Villain, F. *J. Photochem. Photobiol. A* **1994**, *78*, 169.
(19) Villain, F.; Briois, V.; Castro, I.; Helary, C.; Verdaguer, M. *Anal. Chem.* **1993**, *65*, 2545.
(20) Prieto, C.; Lagarde, P.; Dexpert, H.; Briois, V.; Villain, F.; Verdaguer, M. *J. Phys. Chem. Solids* **1992**, *53*, 233.
(21) Prieto, C.; Briois, V.; Parent, P.; Villain, F.; Lagarde, P.; Dexpert, H.; Fourman, B.; Michalowicz, A.; Verdaguer, M. *Conference Proceedings No. 258 Synchrotron Radiation and Dynamic Phenomena*; Beswick, A., Ed.; American Institute of Physics: New York, 1992; p 621.
(22) Bonin, D.; Kaiser, P.; Fretigny, C.; Desbarres, J. In *Structures Fines d'Absorption des Rayons X en Chimie, Vol. 3: Logiciels d'Analyse EXAFS*; Dexpert, H., Michalowicz, A., Verdaguer, M., Eds.; Société Française de Chimie: Paris, France, 1989.
(23) (a) Zhang, D. H.; Brodie, D. E. *Thin Solid Films* **1992**, *213*, 109. (b) Kavan, L.; Stoto, T.; Grätzel, M.; Fitzmaurice, D.; Shklover, V. *J. Phys. Chem.* **1993**, *97*, 9493.
(24) Landolt-Börnstein. *Zahlenwerte und Funktionen aus Naturwissenschaft und Technik*; Springer-Verlag: Berlin, 1982; Vol. III−17g, Section 9.15.2.1.1.
(25) Kormann, C.; Bahnemann, D. W.; Hoffmann, M. R. *J. Phys. Chem.* **1988**, *92*, 5196.
(26) Brus, L. E. *J. Phys. Chem.* **1983**, *79*, 5566.
(27) (a) Henglein, A. *Ber. Bunsen-Ges. Phys. Chem.* **1982**, *86*, 241. (b) Kölle, U.; Moser, J.; Grätzel, M. *Inorg. Chem.* **1985**, *24*, 2253.
(28) Pichat, P.; Herrmann, J.-M.; Disdier, J.; Courbon, H.; Mozzanega, M. N. *Nouv. J. Chim.* **1981**, *5*, 627.
(29) Hénglein, A.; Schnabel, W.; Wendenburg, J. *Einführung in die Strahlenchemie*; Verlag Chemie: Weinhaim, Federal Republic of Germany, 1969; p 168.
(30) Kiwi, J.; Grätzel, M. *J. Mol. Catal.* **1987**, *39*, 63.
(31) Massey, A. G.; Thompson, N. R.; Johnson, B. F. G.; Davis, R. in *The Chemistry of Copper, Silver and Gold*, Pergamon Texts in Inorganic Chemistry, Vol. 17; Pergamon Press: Oxford, 1973.
(32) Clausen, B. S.; Gråbaek, L.; Topsøe, H.; Hansen, L. R.; Stoltze, P.; Nørskov, J. K.; Nielsen, O. H. *J. Catal.* **1993**, *141*, 368.
(33) In ref 15, p 362.
(34) Mason, M. G. *Phys. Rev.* **1983**, *27*, 748.
(35) Herrmann, J.-M.; Disdier, J.; Pichat, P. *J. Catal.* **1988**, *113*, 72.
(36) Sham, T. K.; Yiu, Y. M.; Kuhn, M.; McCuaing, S. In *X-Ray Absorption Fine Structure*; Samar Hasnain, S., Ed.; Ellis Horwood: New York, 1991; p 475.
(37) Lagarde, P.; Morata, T.; Vlaic, G.; Freund, E.; Dexpert, H.; Bournonville, J. P. *J. Catal.* **1983**, *84*, 333.
(38) Disdier, J.; Herrmann, J. M.; Pichat, P. *J. Chem. Soc., Faraday Trans. 1* **1983**, *79*, 651.
(39) Courbon, H.; Herrmann, J. M.; Pichat, P. *J. Phys. Chem.* **1984**, *88*, 5210.

JP9421038